Electronic Supplementary Material (ESI) for ChemComm.

Supporting Information

In Silico Strategy to Boost Stability, Axiality, and Barrier Heights in Dysprocenium SIMs via SWCNT Encapsulation

Rizwan Nabi, Rupesh Kumar Tiwari and Gopalan Rajaraman*†

† Department of Chemistry, Indian Institute of Technology Bombay, Powai, Mumbai-400076, India. Tel: (+91)-22-2576-7183. Email: rajaraman@chem.iitb.ac.in

Table of Contents

Computational details:

All the DFT calculations have been performed in the CP2k program package.[1, 2] The CP2k package utilises a hybrid basis set formalism known as Gaussian and Plane Wave Method[3] (GPW) where the Kohn–Sham orbitals are expanded in terms of contracted Gaussian type orbitals (GTOs), while an auxiliary plane-wave basis set is used to expand the electronic charge density. A double-ζ GTH basis set and their relativistic norm-conserving pseudopotentials (Goedecker, Teter, and Hutter)[4] optimised for PBE were used in addition to a plane wave basis set with an energy cut-off of 450 Ry.[5] All calculations were carried out with DZVP-MOLOPT-GTH (valence double-zeta (ζ) plus polarisation, molecularly optimised, Goedecker-Teter-Hutter) basis set for all atoms (H, C,) and DZVP-MOLOPT-SR-GTH (valence double-zeta (ζ) plus polarisation, molecularly optimised, short-range Goedecker-Teter-Hutter) basis set for Y as implemented in the CP2k.[3] The pseudopotential used was GTH-pseudopotential (Goedecker-Teter-Hutter). PBE functional has been used throughout the calculations performed with the CP2k package. To account for dispersion, the DFT-D2 approach implemented in CP2k has been used throughout the calculations. All the ab initio calculations have been performed by the post-Hartree–Fock *ab initio* calculations by using the MOLCAS 8.0 code.[6] Basis sets for all atoms were taken from the ANO-RCC library as implemented in the MOLCAS package.

Table S1. List of the used ANO-RCC basis sets.

Element	*Basis Sets*	
Dy	8s7p5d3f2g1h.	ANO-RCC-VTZP
C	3s2p1d.	ANO-RCC-VDZP
C (SWCNT)	3s2p1d.	ANO-RCC-VDZ
H	2s1p.	ANO-RCC-VDZ

All the calculations were carried out using complete active space (CAS). In the case of Dy, the active space comprised of nine active electrons of Dy^{III} in the seven 4f active orbitals RAS (9,7). The ground-state *f*-electron configuration for Dy^{III} is found to be $4f^9$, which yields $^6H_{15/2}$ multiplet as the ground state. The CASSCF calculations were performed with the same basis sets and active spaces to obtain relative energies of the Kramers doublets (KDs), *g* tensors. For Dy^{III}, we used 21

roots in the sextet state and 128 roots in the quartet state in the configuration interaction (CI) procedure. Once these spin-free excited states are obtained, we mixed all of these states by using the RASSI-SO module to compute the spin-orbit coupled states. We obtained eight low-lying KDs for Dy^{III} ion which finally yielded *g*-tensors. All the frequency calculations were carried out in Gaussian 09 program package. For all the elements, TZV basis sets and B3LYP functional[7] were used for all the calculations implemented in Gaussian 09.[8]

Here, we are using metallic armchair SWCNTs to investigate their effect on the magnetic properties of dysprocenium SIMs. We are using two types of SWCNTs. For model complex **1**, we are using CNT(7,7) in both the arrangements parallel ($1^{\parallel}$@CNT) as well as perpendicular ($1^{\perp}$@CNT) having diameter and length of ~8.5 and ~11.0 Å respectively. For complexes **2** and **3**, we are using CNT(10,10) having diameter and length of ~6.8 and ~12.3 Å respectively. For model complex Dy@ stones-wale defected SWCNT) we are using CNT(3,3) having diameter and length 5.35 Å and 10 Å respectively. The CNT(10,10) SWCNT was experimentally synthesized and has been studied widely for use in Li-ion batteries.[9-11] There are also many reports on SWCNTs like CNT(7,7) and CNT(3,3).[12, 13]

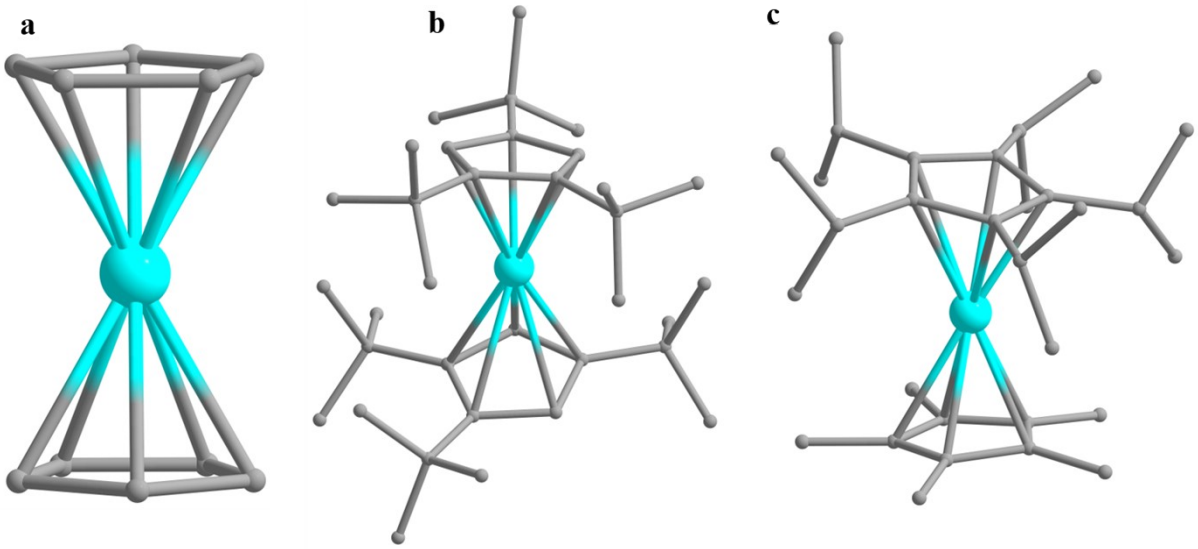

Figure S1: Optimised molecular structure of various dysprosocenium complexes. a.) model $[DyCp_2]^+$ (**1**) **b.)** $[Dy(Cp^{ttt})_2]^+$ (**2**) **c.)** $[(Cp^{ipr5})Dy(Cp^*)]$ (**3**); Where, (*Cp^{ttt}=1,2,4-tri(tertbutyl) cyclopentadienide), (*Cp^{iPr5} = penta-iso-propylcyclopentadienyl, Cp* = pentamethylcyclopentadienyl).*

Table S2. Dy-C bond lengths and Cp-Dy-Cp angle of $\mathbf{2_{opt}}$, $\mathbf{2_{x\text{-}ray}}$, $\mathbf{3_{opt}}$, $\mathbf{3_{x\text{-}ray}}$

	$\mathbf{2_{opt}}$	$\mathbf{2_{x\text{-}ray}}$	$\mathbf{3_{opt}}$	$\mathbf{3_{x\text{-}ray}}$
Dy-C1	2.554	2.491	2.597	2.587
Dy-C2	2.614	2.706	2.545	2.634
Dy-C3	2.616	2.627	2.590	2.534

Dy-C4	2.480	2.345	2.534	2.417
Dy-C5	2.585	2.288	2.523	2.457
Dy-C6	2.579	2.234	2.594	2.399
Dy-C7	2.624	2.399	2.601	2.596
Dy-C8	2.573	2.642	2.593	2.682
Dy-C9	2.593	2.702	2.589	2.558
Dy-C10	2.522	2.480	2.587	2.392
Cp-Dy-Cp	162.151	180	176.261	180

Table S3. CASSCF+RASSI-SO computed energies of KDs and SINGLE_ANISO computed *g*-tensors of $\mathbf{2}_{opt}$, $\mathbf{2}_{x\text{-}ray}$, $\mathbf{3}_{opt}$, $\mathbf{3}_{x\text{-}ray}$.

KDs	E(cm^{-1})	g_x	g_y	g_z	θ
		$\mathbf{2}_{opt}$			
15/2	0.0	0.000	0.000	20.022	~
13/2	551.38	0.000	0.000	17.025	0.389
11/2	817.89	0.006	0.006	14.477	0.881
9/2	961.43	0.013	0.026	11.862	1.305
7/2	1107.83	0.551	0.572	9.102	1.073
5/2	1273.44	0.221	1.274	6.318	1.194
3/2	1420.85	7.179	5.339	3.258	1.752
1/2	1543.32	0.794	3.820	16.287	90.12
		$\mathbf{2}_{x\text{-}ray}$			
15/2	0.0	0.000	0.000	20.040	~
13/2	690.06	0.000	0.000	16.958	1.688
11/2	952.61	0.002	0.003	14.607	6.975
9/2	1040.94	0.072	0.078	12.069	6.116
7/2	1168.13	0.154	0.270	9.162	5.670
5/2	1353.74	3.824	4.223	5.961	6.670
3/2	1574.57	2.965	3.329	4.981	90.986
1/2	1704.57	11.488	9.504	1.147	0.249
		$\mathbf{3}_{opt}$			

15/2	0.0000	0.000	0.000	20.010	~
13/2	665.11	0.000	0.000	16.933	0.786
11/2	952.03	0.012	0.012	14.466	2.584
9/2	1073.91	0.016	0.040	11.884	2.026
7/2	1219.15	0.285	0.337	9.104	2.630
5/2	1409.87	0.164	0.456	6.315	1.888
3/2	1599.48	3.390	3.542	3.945	89.897
1/2	1732.60	1.069	6.740	14.061	89.987
		$3_{\text{x-ray}}$			
15/2	0.0000	0.000	0.000	20.010	~
13/2	688.26	0.000	0.000	16.924	1.896
11/2	972.47	0.024	0.025	14.501	5.261
9/2	1084.90	0.007	0.039	11.996	6.251
7/2	1227.00	0.047	0.076	9.162	6.215
5/2	1423.94	0.286	0.426	6.323	4.386
3/2	1626.72	1.403	2.082	3.634	5.546
1/2	1761.87	12.245	8.748	1.161	0.759

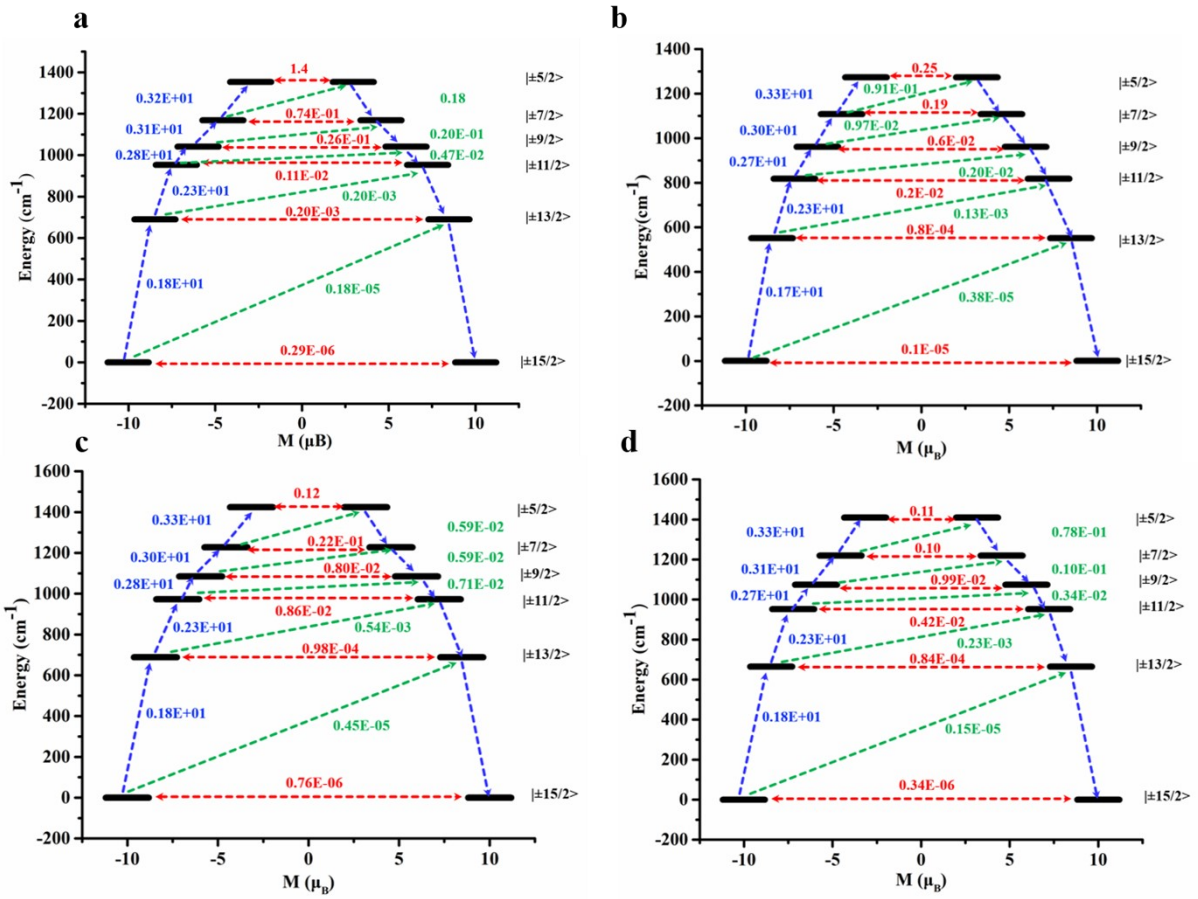

Figure S2: A*b initio* computed magnetisation blockade barriers, along with computed transversal magnetic moments between the connecting pairs for complexes $\mathbf{2}_{\mathbf{opt}}$, $\mathbf{2}_{\mathbf{x\text{-}ray}}$, $\mathbf{3}_{\mathbf{opt}}$, $\mathbf{3}_{\mathbf{x\text{-}ray}}$.

Binding Energy

The binding energy of the title complexes in SWCNT has been determined by using the equation shown below.

$$\Delta E = \{E_{Dy@SWCNT}\} - \{E_{SWCNT} + E_{Dy}\}$$

Where ΔE is the binding energy, $E_{\mathrm{Dy@SWCNT}}$ is the energy of the complex in SWCNT; E_{SWCNT} is the energy of SWCNT whereas E_{Dy} is the energy of optimized geometry of the title complexes.

Table S4. Binding energy of the title complexes inside SWCNT.

Geometry	*Binding Energy (kJmol^{-1})*
1$^{\parallel}$@CNT	-858.1
1$^{\perp}$@CNT	-594.5
2$^{\parallel}$@CNT	-983.6
3$^{\parallel}$@CNT	-855.2

Table S5. C-H vibrational frequencies of different C-H bonds of the **1**, **1$^{\parallel}$@CNT** and **2** along with experimentally observed values for **2**.

1	**2**	**1$^{\parallel}$@CNT**	**2 (Reported)**
3146.2	-	3303.1	-
3147.3	-	3306.9	-
3148.7	-	3317.2	-
3149.1	-	3346.1	-
3159.9	-	3356.2	-
3160.6	-	3365.5	-
3162.4	3162.5	3380.9	3181.2
3162.9	3163.9	3388.9	3181.3
3172.4	3185.4	3399.9	3181.3
3172.6	3189.8	3420.5	3181.4

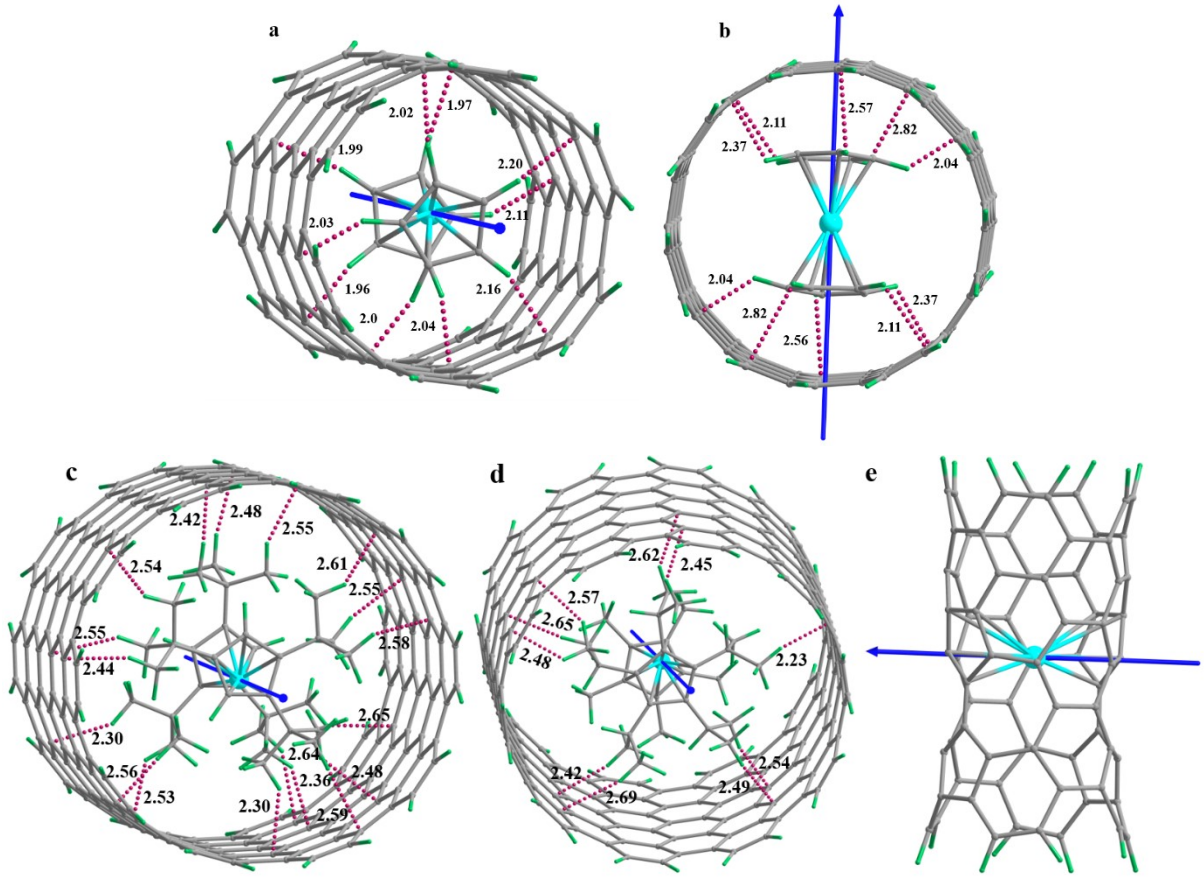

Figure S3. DFT optimised structures (**a) 1^{II}@CNT (b) 1$^{\perp}$@CNT** (**c) 2^{II}@CNT** and **(d**) **3^{II}@CNT (e)** model Dy^{III} ion incorporated inside SWCNT. Dotted purple lines show the closest C-H bond distances. Colour code: Dy^{III} - cyan, C- grey, and H- green. Blueline arrow shows the ground state g_{zz} axis.

Table S6. CASSCF+RASSI-SO computed energies of all low-lying KDs, and SINGLE_ANISO computed *g*-tensors of **1**$^{\parallel}$**@CNT** and **1**$^{\perp}$**@CNT**

KDs	E(cm^{-1})	g_x	g_y	g_z	θ
		1$^{\parallel}$**@CNT**			
1	0.0	0.000	0.000	19.938	~
2	563.97	0.000	0.000	17.005	0.4
3	809.73	0.014	0.014	14.457	1.9
4	946.26	0.007	0.019	11.843	1.8
5	1097.11	0.115	0.127	9.115	2.6
6	1274.09	0.298	0.532	6.386	2.3
7	1440.03	0.444	1.276	3.747	3.3
8	1542.74	11.373	9.654	1.228	0.2
		1$^{\perp}$**@CNT**			
1	0.0	0.000	0.000	19.907	~
2	781.12	0.009	0.012	16.769	3.8
3	1018.68	0.103	0.171	14.261	14.0
4	1091.54	0.018	0.282	12.241	13.3
5	1211.51	0.206	0.490	9.869	15.1
6	1394.95	1.295	1.977	6.409	9.2
7	1600.21	3.307	3.881	7.259	89.3
8	1767.31	0.899	4.643	15.771	90.9

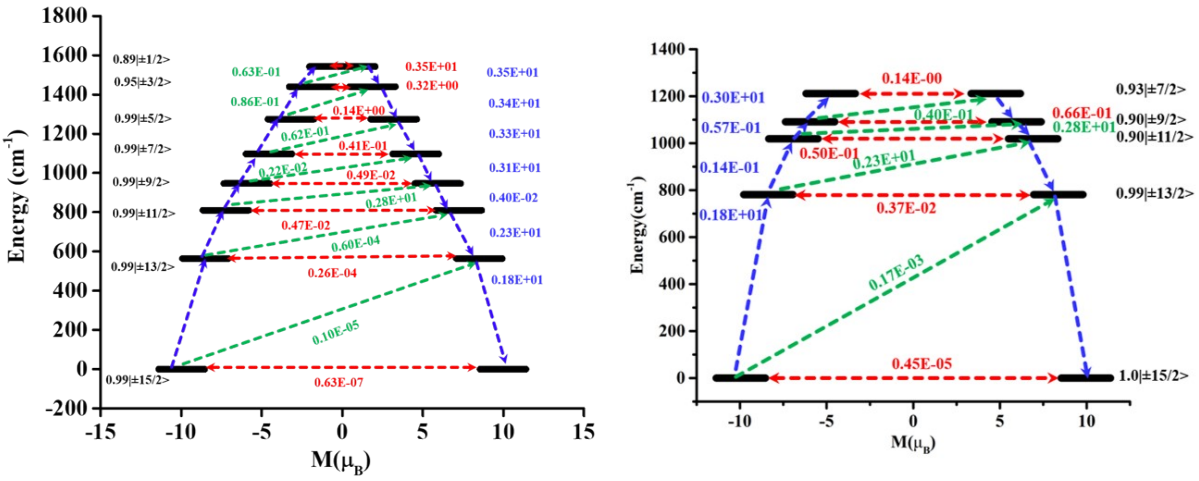

Figure S4: *Ab initio* computed magnetisation blockade barriers, along with computed transversal magnetic moments between the connecting pairs for complexes **1$^{\parallel}$@CNT** and **1$^{\perp}$@CNT**.

Table S7. CASSCF+RASSI-SO computed energies of all low-lying KDs, and SINGLE_ANISO computed *g*-tensors of **2$^{\parallel}$@CNT** and **3$^{\parallel}$@CNT**

KDs	E(cm^{-1})	g_{xx}	g_{yy}	g_{zz}	θ
		2$^{\parallel}$@CNT			
1	0.0	0.000	0.000	19.953	~
2	413.9	0.000	0.000	17.081	1.5
3	661.6	0.007	0.008	14.466	2.4
4	822.9	0.039	0.052	11.797	0.9
5	964.6	0.431	0.587	9.126	1.3
6	1082.5	3.058	4.430	5.908	1.1
7	1163.4	2.114	5.775	11.007	90.0
8	1293.5	0.114	0.264	18.308	89.9
		3$^{\parallel}$@CNT			
1	0.0	0.000	0.000	19.910	~
2	487.4	0.000	0.000	17.028	0.8

3	749.4	0.006	0.007	14.401	1.2
4	910.8	0.049	0.059	11.748	1.4
5	1061.3	0.313	0.435	09.118	0.9
6	1205.3	0.092	0.609	06.466	0.8
7	1314.8	6.986	5.953	03.294	1.8
8	1404.2	0.743	3.299	16.258	89.8

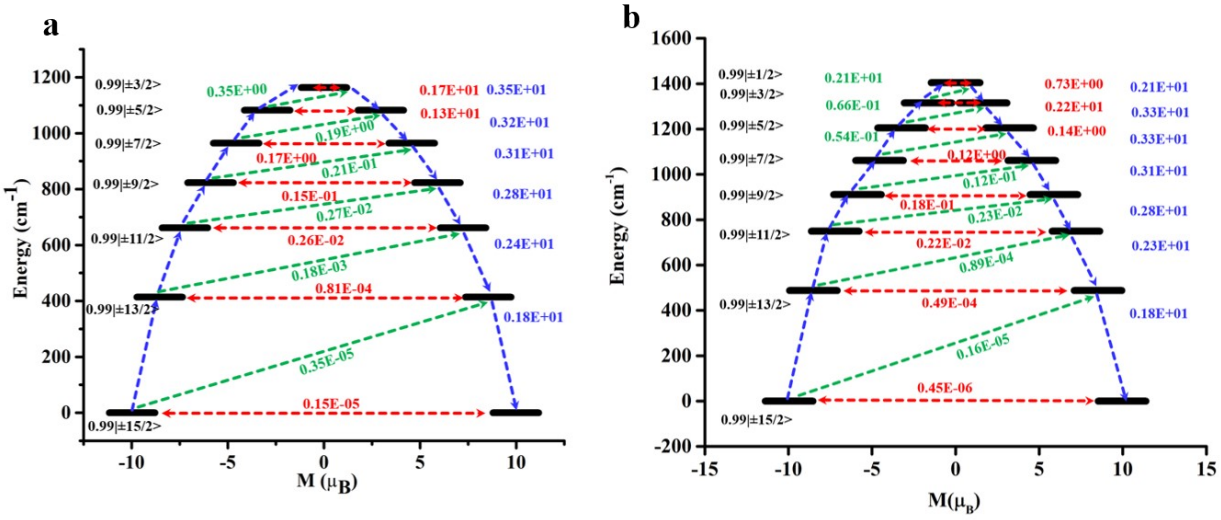

Figure S5: *Ab initio* computed magnetisation blockade barriers, along with computed transversal magnetic moments between the connecting pairs for complexes **2^{II}@CNT** and **3^{II}@CNT**.

Table S8. CASSCF+RASSI-SO computed energies of all low-lying KDs, and SINGLE_ANISO computed *g*-tensors of **model Dy ion inbuilt complex.**

KDs	E(cm-1)	g_{xx}	g_{yy}	g_{zz}	θ
1	0.00	0.001	0.006	19.34	~
2	91.31	1.398	3.335	13.504	2.4
3	146.77	4.123	5.098	7.001	13.7
4	229.94	2.213	2.751	8.932	89.9
5	341.14	0.006	1.084	11.53	89.9
6	453.16	0.468	0.536	14.149	89.9
7	566.67	0.049	0.135	16.792	89.9
8	660.16	0.06	0.084	19.539	89.9

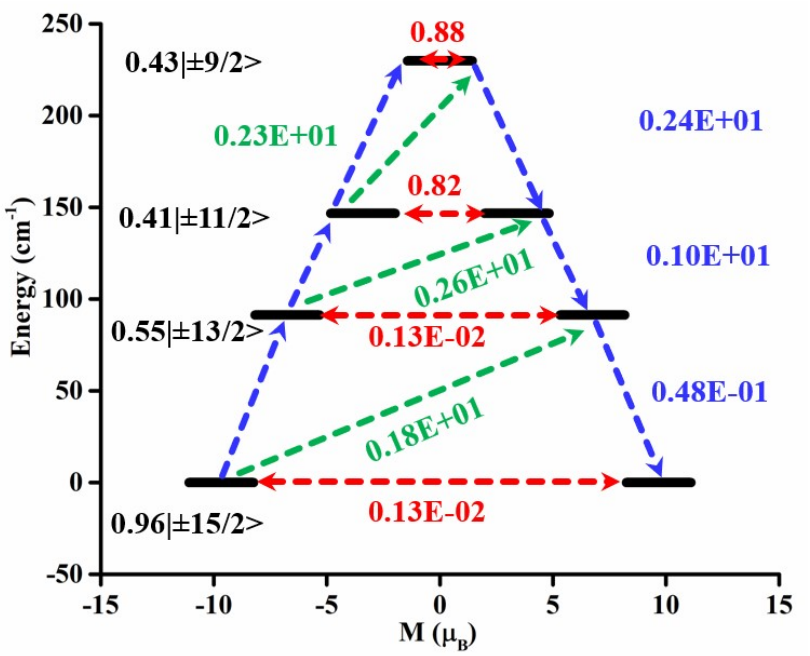

Figure S6. A*b initio* computed magnetisation blockade barriers, along with computed transversal magnetic moments between the connecting pairs for **model Dy ion inbuilt complex.**

Table S9. Comparison of energy barrier of the title complexes.

Geometry	Calculated energy barrier (U_{cal}) (cm^{-1})			Effective energy barrier (U_{eff}) (cm^{-1}) (reported)
	optimised	**Inside CNT**	**XRAY/Model Str.**	
1	-	-	921.3	-
2	1273	-	1354	1277
3	1409	-	1424	1541
$1^{||}$@CNT	-	1543	-	-
$1^{\perp}$@CNT	-	1211	-	-
$2^{||}$@CNT	-	1163	-	-
$3^{||}$@CNT	-	1404	-	-
model Dy ion inbuilt complex	-	230	-	-

LoProp Charges

Table S10. LoProp charges on atoms of molecule **1** without SWCNT and with SWCNT and the difference (**Δδ**)

Atom	**1**	**1||@CNT**		**$1^{\perp}$@CNT**	
	Charge	Charge	Δδ	Charge	Δδ
Dy	2.355	2.363	0.008	2.460	0.105
C1	-0.276	-0.243	0.033	-0.315	-0.039
C2	-0.273	-0.315	-0.042	-0.320	-0.047
C3	-0.268	-0.341	-0.073	-0.256	-0.012
C4	-0.271	-0.388	-0.117	-0.298	-0.027
C5	-0.272	-0.235	0.037	-0.304	-0.032

C6	-0.271	-0.329	-0.058	-0.298	-0.027
C7	-0.272	-0.304	-0.032	-0.304	-0.032
C8	-0.277	-0.327	-0.050	-0.315	-0.038
C9	-0.273	-0.340	-0.067	-0.320	-0.047
C10	-0.268	-0.261	0.007	-0.256	0.012
H1	0.136	0.122	-0.014	0.127	-0.009
H2	0.136	0.110	-0.026	0.110	-0.026
H3	0.137	0.110	-0.027	0.134	-0.003
H4	0.137	0.119	-0.018	0.130	-0.007
H5	0.137	0.114	-0.023	0.112	-0.025
H6	0.137	0.122	-0.015	0.130	-0.007
H7	0.137	0.129	-0.008	0.112	-0.025
H8	0.136	0.119	-0.017	0.127	-0.009
H9	0.136	0.111	-0.025	0.110	-0.026
H10	0.137	0.122	-0.015	0.134	-0.003

Table S11. LoProp charges on atoms of molecules **2** and **3** without SWCNT and with SWCNT and the difference (**Δδ**)

Atom	**2**	**2||@CNT**	**3**	**3||@CNT**
Dy	2.299	2.291	2.412	2.296
C1	-0.212	-0.184	-0.132	-0.1925
C2	-0.298	-0.318	-0.151	-0.2115
C3	-0.138	-0.131	-0.143	-0.1799
C4	-0.342	-0.298	-0.1668	-0.1627
C5	-0.165	-0.168	-0.1463	-0.1830
C6	-0.217	-0.193	-0.1565	-0.1624
C7	-0.164	-0.171	-0.2028	-0.1506
C8	-0.337	-0.310	-0.2125	-0.1234
C9	-0.299	-0.112	-0.2486	-0.1854
C10	-0.123	-0.305	-0.2269	-0.1422
C	-0.364	-0.274	-0.2687	-0.2870
C	-0.358	-0.278	-0.2731	-0.2892
C	-0.366	-0.283	-0.2742	-0.2947
C	0.087	0.062	-0.2760	-0.2979

C	-0.357	-0.279	-0.2737	-0.2910
C	-0.371	-0.286	-0.0374	-0.0469
C	-0.365	-0.290	-0.2600	-0.2963
C	0.100	0.079	-0.2701	-0.2872
C	-0.358	-0.280	-0.0356	-0.0489
C	-0.395	-0.291	-0.2593	-0.2907
C	-0.363	-0.284	-0.2624	-0.2792
C	0.091	0.070	-0.0326	-0.0450
C	-0.368	-0.281	-0.2846	-0.3242
C	-0.364	-0.282	-0.2619	-0.2800
C	-0.357	-0.283	-0.0327	-0.0412
C	0.087	0.067	-0.2658	-0.2843
C	-0.370	-0.286	-0.2562	-0.2858
C	-0.355	-0.283	-0.0323	-0.0418
C	-0.365	-0.286	-0.2627	-0.2804
C	0.096	0.079	-0.2653	-0.2854
C	-0.358	-0.316		
C	-0.394	-0.289		
C	-0.362	-0.282		
C	0.089	0.072		
H	0.123	0.104	0.1117	0.1100
H	0.123	0.097	0.0872	0.0960
H	0.129	0.098	0.1002	0.1018
H	0.131	0.104	0.1160	0.1143
H	0.125	0.102	0.1013	0.1043
H	0.103	0.047	0.0866	0.0892
H	0.126	0.033	0.0854	0.0806
H	0.123	0.109	0.1145	0.1189
H	0.122	0.097	0.1015	0.1098
H	0.119	0.098	0.0865	0.0799
H	0.129	0.081	0.1025	0.1102
H	0.107	0.099	0.1140	0.1210
H	0.119	0.072	0.1141	0.1146
H	0.110	0.094	0.0944	0.0942
H	0.128	0.087	0.0992	0.1059

H	0.134	0.096	0.0862	0.1001
H	0.134	0.097	0.1006	0.1041
H	0.121	0.084	0.0875	0.0905
H	0.086	0.100	0.1013	0.1049
H	0.117	0.100	0.0834	0.0771
H	0.126	0.088	0.1087	0.1113
H	0.150	0.093	0.0432	0.0628
H	0.134	0.098	0.0877	0.1028
H	0.091	0.068	0.0983	0.1062
H	0.113	0.097	0.0843	0.0906
H	0.120	0.084	0.0965	0.1011
H	0.130	0.096	0.0892	0.0985
H	0.135	0.092	0.1031	0.1142
H	0.135	0.119	0.0463	0.0298
H	0.102	0.030	0.0894	0.0994
H	0.131	0.096	0.0980	0.1041
H	0.125	0.100	0.0851	0.0933
H	0.123	0.068	0.0952	0.0968
H	0.129	0.094	0.0742	0.0966
H	0.103	0.100	0.1089	0.1206
H	0.120	0.093	0.0738	0.0605
H	0.087	0.099	0.0796	0.0944
H	0.120	0.101	0.0409	0.0632
H	0.134	0.080	0.0936	0.0883
H	0.119	0.088	0.1016	0.0952
H	0.129	0.087	0.0959	0.0986
H	0.124	0.092	0.0898	0.0960
H	0.122	0.090	0.0970	0.0989
H	0.121	0.091	0.0846	0.0892
H	0.129	0.086	0.0463	0.0736
H	0.122	0.087	0.0874	0.0869
H	0.112	0.083	0.1083	0.0922
H	0.103	0.062	0.0859	0.0925
H	0.090	0.085	0.0937	0.0996
H	0.150	0.114	0.0989	0.0979

H	0.110	0.102		
H	0.132	0.126		
H	0.129	0.082		
H	0.118	0.084		
H	0.133	0.083		
H	0.126	0.103		
H	0.135	0.123		
H	0.134	0.122		

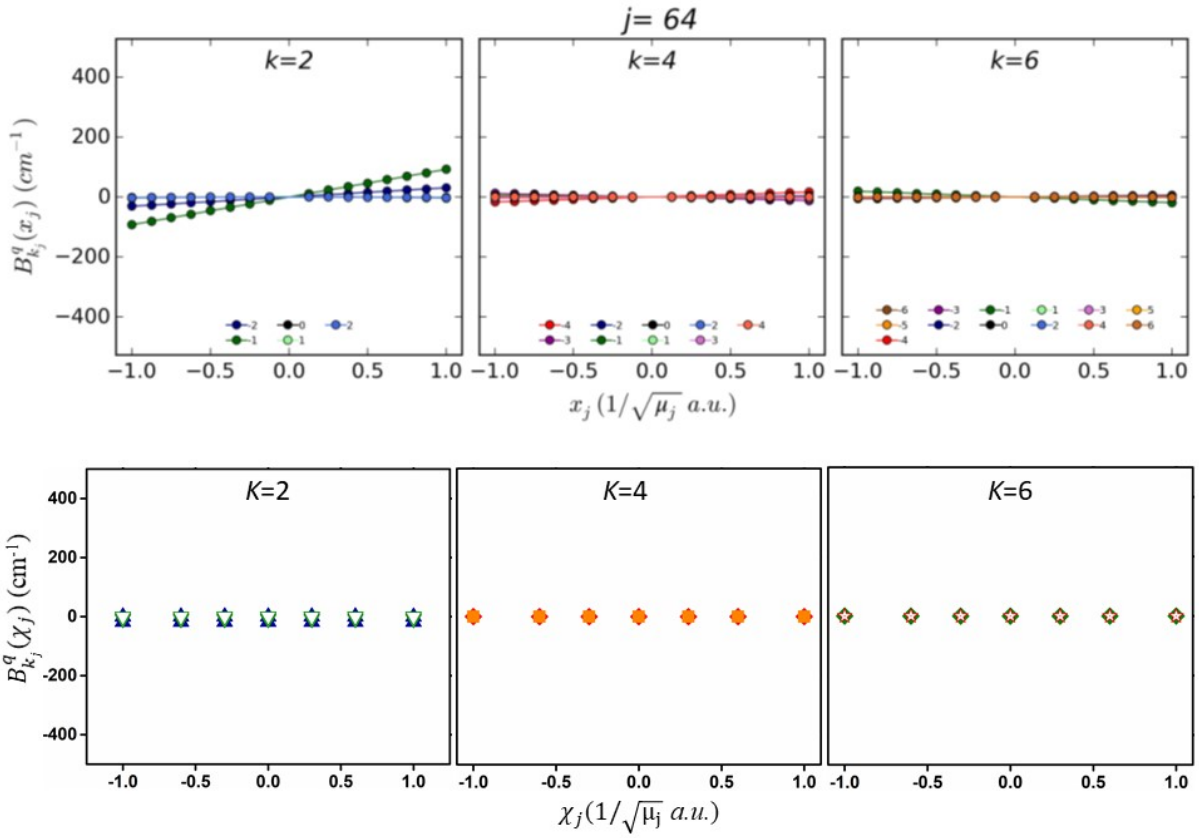

Figure S7a. Plots showing the crystal filed parameters for the complex **1||@CNT**

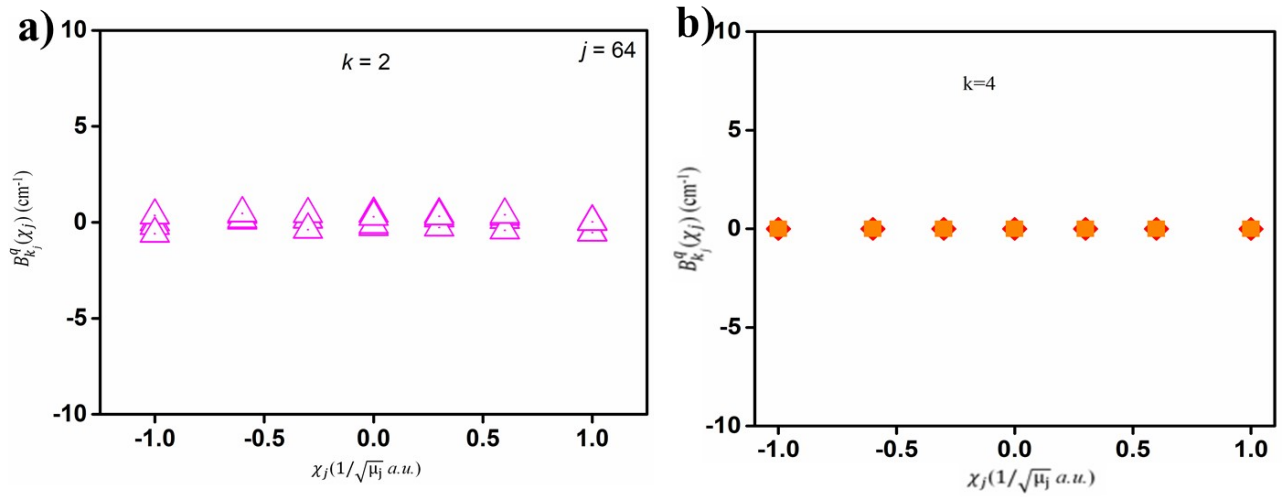

Figure S7b. Plots showing the crystal filed parameters for the complex **1||@CNT**

Table S12. CASSCF+RASSI-SO computed energies of all low-lying KDs, and SINGLE_ANISO computed *g*-tensors of of **1||@CNT** at the displacement, $\chi_j\left(\frac{1}{\sqrt{\mu_j}}a.u.\right) = 0.00$, **0.3, 0.6, 1.0, (-0.3), (-0.6)** and **(-1.0)**.

KDs	E(cm^{-1})	g_{xx}	g_{yy}	g_{zz}
		$\chi_j\left(\frac{1}{\sqrt{\mu_j}}a.u.\right) = 0.00$		
1	0.0	0.000	0.000	20.007
2	553.5	0.000	0.000	17.020
3	792.0	0.018	0.019	14.499
4	912.8	0.012	0.023	11.885
5	1053.6	0.048	0.059	9.123
6	1228.0	0.377	0.476	6.362
7	1397.8	0.370	1.224	3.711
8	1505.7	11.352	9.753	1.212

$$\chi_j\left(\frac{1}{\sqrt{\mu_j}}a.u.\right) = 0.3$$

1	0.0	0.000	0.000	20.007
2	552.1	0.000	0.000	17.023
3	790.2	0.018	0.019	14.500
4	911.4	0.012	0.024	11.900
5	1051.8	0.060	0.072	09.138
6	1225.6	0.682	0.808	06.359
7	1395.4	0.362	1.811	03.701
8	1503.1	11.621	9.477	1.207

$$\chi_j\left(\frac{1}{\sqrt{\mu_j}}a.u.\right) = 0.6$$

1	0.0	0.000	0.000	20.007
2	553.0	0.000	0.000	17.021
3	791.4	0.018	0.019	14.500
4	912.3	0.012	0.023	11.889
5	1053.0	0.050	0.006	9.127
6	1227.3	0.450	0.553	6.362
7	1397.1	0.314	1.315	3.710
8	1504.9	11.370	9.736	1.212

$$\chi_j\left(\frac{1}{\sqrt{\mu_j}}a.u.\right) = 1.0$$

1	0.0	0.000	0.000	20.007
2	552.6	0.000	0.000	17.022
3	790.8	0.018	0.019	14.500
4	911.9	0.012	0.023	11.893

5	1052.5	0.053	0.064	09.131
6	1226.6	0.542	0.652	06.361
7	1396.3	0.298	1.490	03.707
8	1504.1	11.449	9.655	1.211

$$\chi_j\left(\frac{1}{\sqrt{\mu_j}}a.u.\right) = -\,0.3$$

1	0.0	0.000	0.000	20.007
2	555.5	0.000	0.000	17.016
3	794.3	0.019	0.019	14.494
4	914.5	0.012	0.023	11.875
5	1055.4	0.048	0.059	09.116
6	1230.1	0.388	0.491	06.358
7	1400.4	0.724	1.620	03.701
8	1509.0	11.719	9.372	1.205

$$\chi_j\left(\frac{1}{\sqrt{\mu_j}}a.u.\right) = -\,0.6$$

1	0.0	0.000	0.000	20.007
2	554.0	0.000	0.000	17.019
3	792.6	0.018	0.019	14.498
4	913.3	0.012	0.023	11.881
5	1054.1	0.047	0.058	09.120
6	1228.7	0.335	0.433	06.361
7	1398.6	0.462	1.233	03.710
8	1506.6	11.401	9.702	1.211

$$\chi_j\left(\frac{1}{\sqrt{\mu_j}}a.u.\right) = -\,1.0$$

1	0.0	0.000	0.000	20.007
2	554.6	0.000	0.000	17.018
3	793.3	0.019	0.019	14.497
4	913.8	0.012	0.023	11.878
5	1054.6	0.047	0.058	09.118
6	1229.3	0.332	0.432	06.360
7	1399.4	0.572	1.344	03.707
8	1507.6	11.510	9.590	1.209

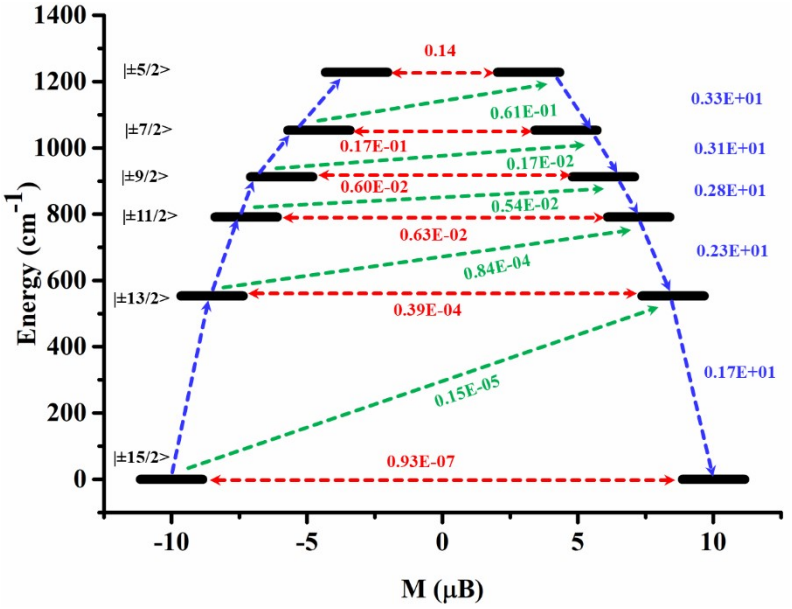

Figure S8: A*b initio* computed magnetisation blockade barriers, along with computed transversal magnetic moments between the connecting pairs for complex **1||@CNT** at a displacement of $\chi_j\left(\frac{1}{\sqrt{\mu_j}}a.u.\right) = 0.0$

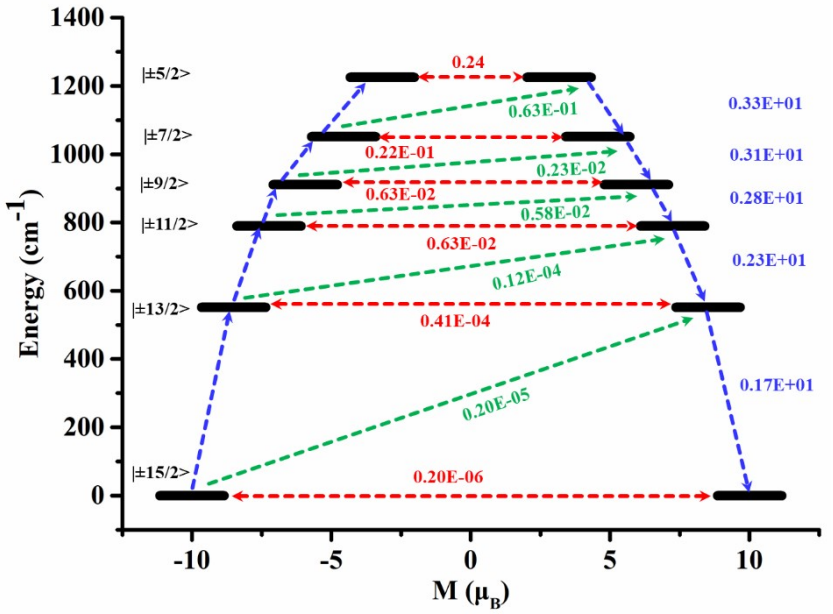

Figure S9: A*b initio* computed magnetisation blockade barriers, along with computed transversal magnetic moments between the connecting pairs for complex **1||@CNT** at a displacement of $\chi_j\left(\frac{1}{\sqrt{\mu_j}}a.u.\right) = 0.3$

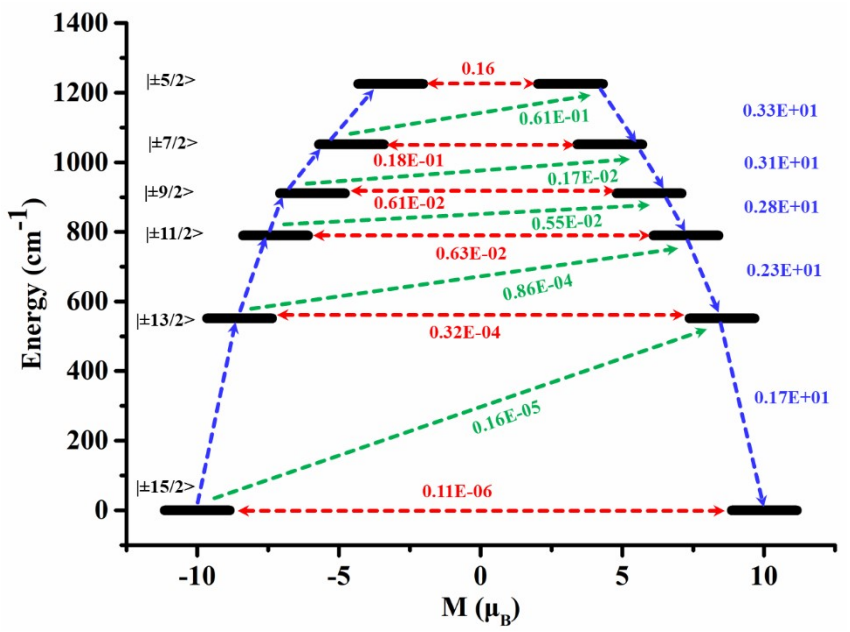

Figure S10: A*b initio* computed magnetisation blockade barriers, along with computed transversal magnetic moments between the connecting pairs for complex **1||@CNT** at a displacement of $\chi_j\left(\frac{1}{\sqrt{\mu_j}}a.u.\right) = 0.6$

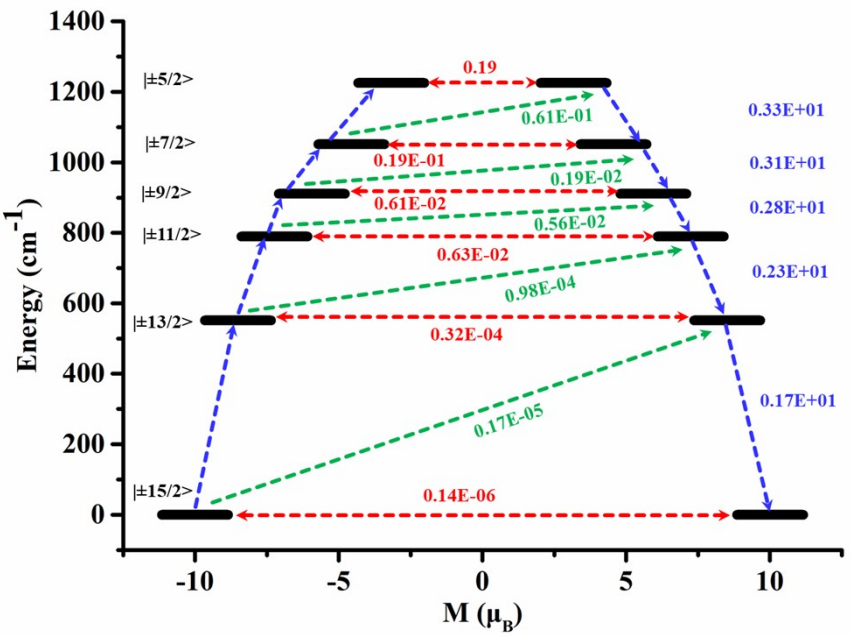

Figure S11: A*b initio* computed magnetisation blockade barriers, along with computed transversal magnetic moments between the connecting pairs for complex **1||@CNT** at a displacement of $\chi_j\left(\frac{1}{\sqrt{\mu_j}}a.u.\right) = 1.0$

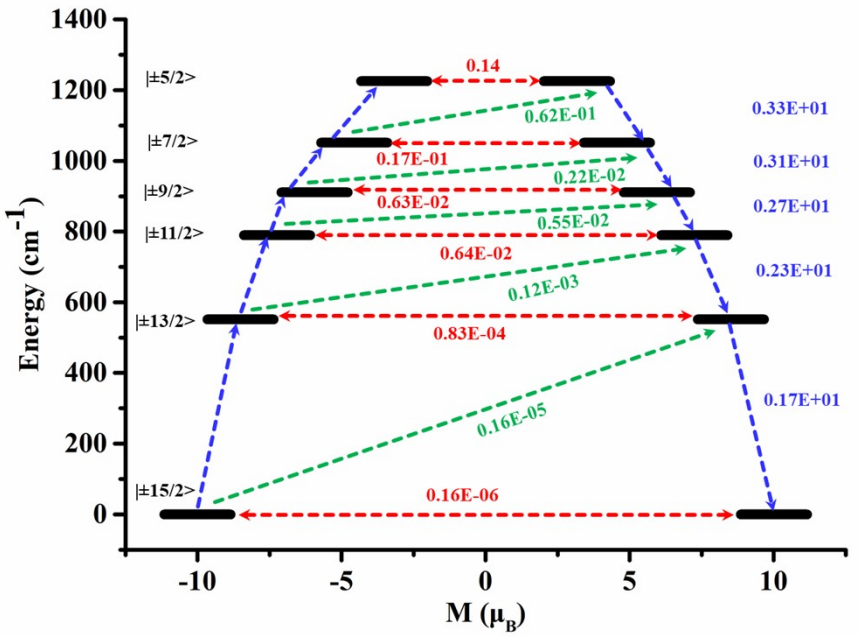

Figure S12: *Ab initio* computed magnetisation blockade barriers, along with computed transversal magnetic moments between the connecting pairs for complex **1||@CNT** at a displacement of $\chi_j\left(\frac{1}{\sqrt{\mu_j}}a.u.\right)$ =– 0.3

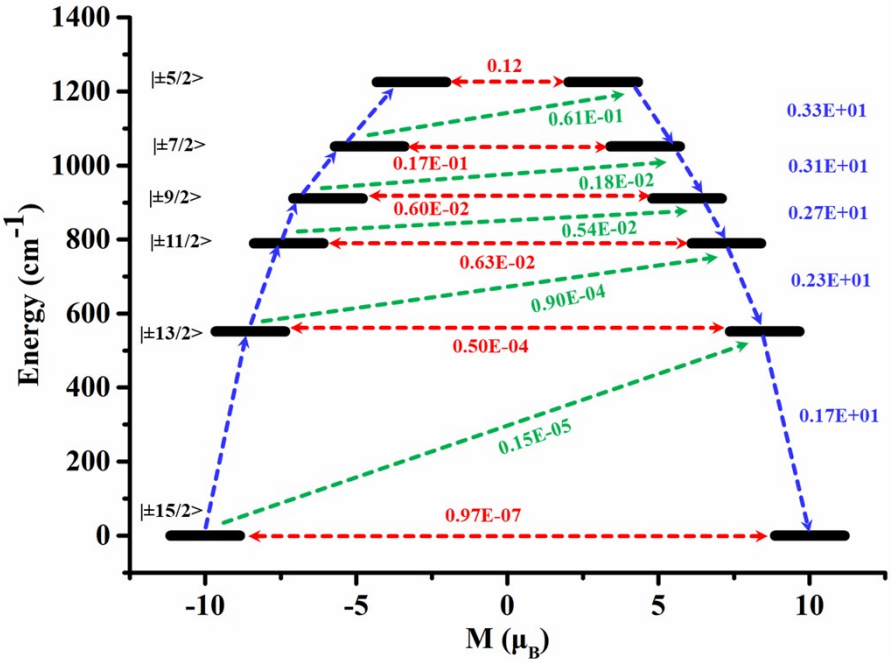

Figure S13: A*b initio* computed magnetisation blockade barriers, along with computed transversal magnetic moments between the connecting pairs for complex **1||@CNT** at a displacement of $\chi_j\left(\frac{1}{\sqrt{\mu_j}}a.u.\right) = -0.6$

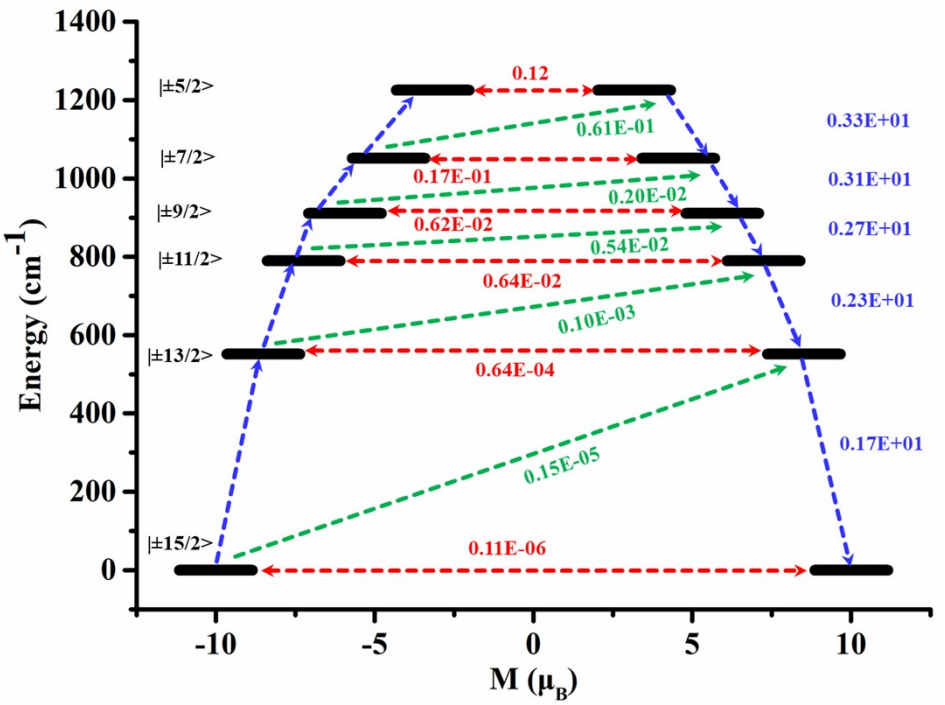

Figure S14: A*b initio* computed magnetisation blockade barriers, along with computed transversal magnetic moments between the connecting pairs for complex **1||@CNT** at a displacement of $\chi_j\left(\frac{1}{\sqrt{\mu_j}}a.u.\right) = -1.0$

Table S13. CASSCF+RASSI-SO computed energies of all low-lying KDs, and SINGLE_ANISO computed *g*-tensors of **2-CA‖@CNT.**

KDs	E(cm-1)	g_{xx}	g_{yy}	g_{zz}
1	0.00	0.000	0.000	20.148
2	419.3	0.000	0.000	17.162
3	670.7	0.002	0.002	14.521
4	834.0	0.017	0.021	11.857
5	980.3	0.230	0.307	9.189
6	1107.9	2.751	3.579	6.123
7	1198.2	2.381	6.246	10.562
8	1327.4	0.200	0.546	18.240

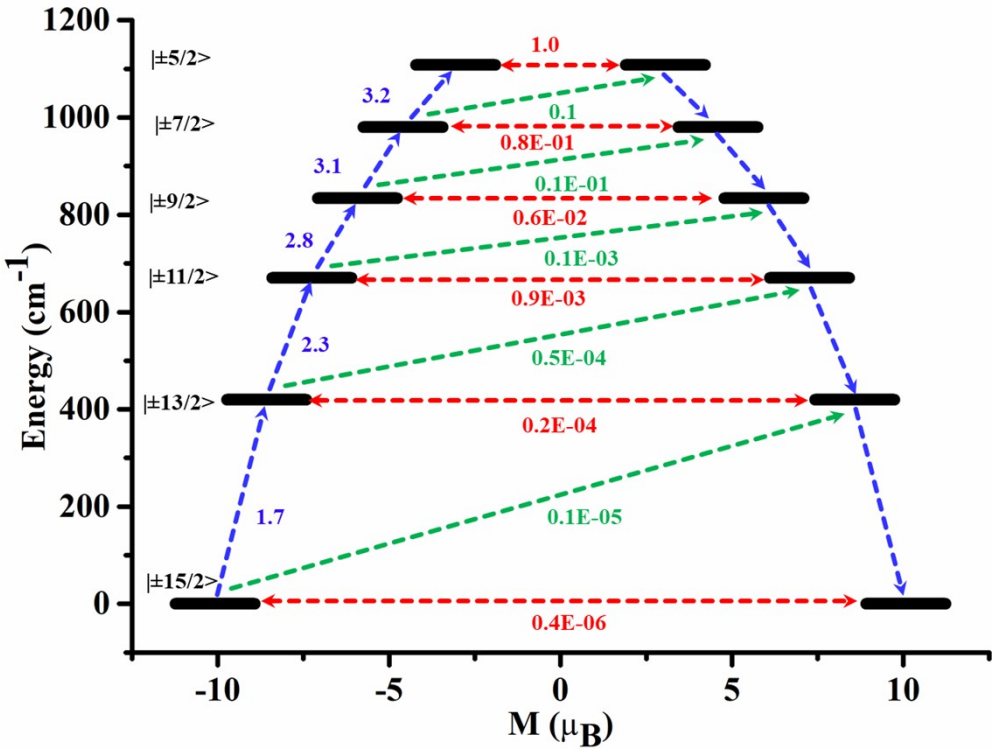

Figure S15. *Ab initio* computed magnetisation blockade barriers, along with computed transversal magnetic moments between the connecting pairs for **2-CA^{II}@CNT.**

Table S14. CASSCF+RASSI-SO computed energies of all low-lying KDs, and SINGLE_ANISO computed *g*-tensors of **3-CA^{II}@CNT.**

KDs	E(cm-1)	g_{xx}	g_{yy}	g_{zz}
1	0.00	0.000	0.000	20.000
2	522.5	0.000	0.000	17.308
3	784.8	0.002	0.002	14.453
4	934.3	0.014	0.018	11.818
5	1084.2	0.006	1.084	11.538
6	1245.7	0.061	0.384	6.417

7	1387.3	3.370	3.616	4.347
8	1482.2	1.067	6.483	14.147

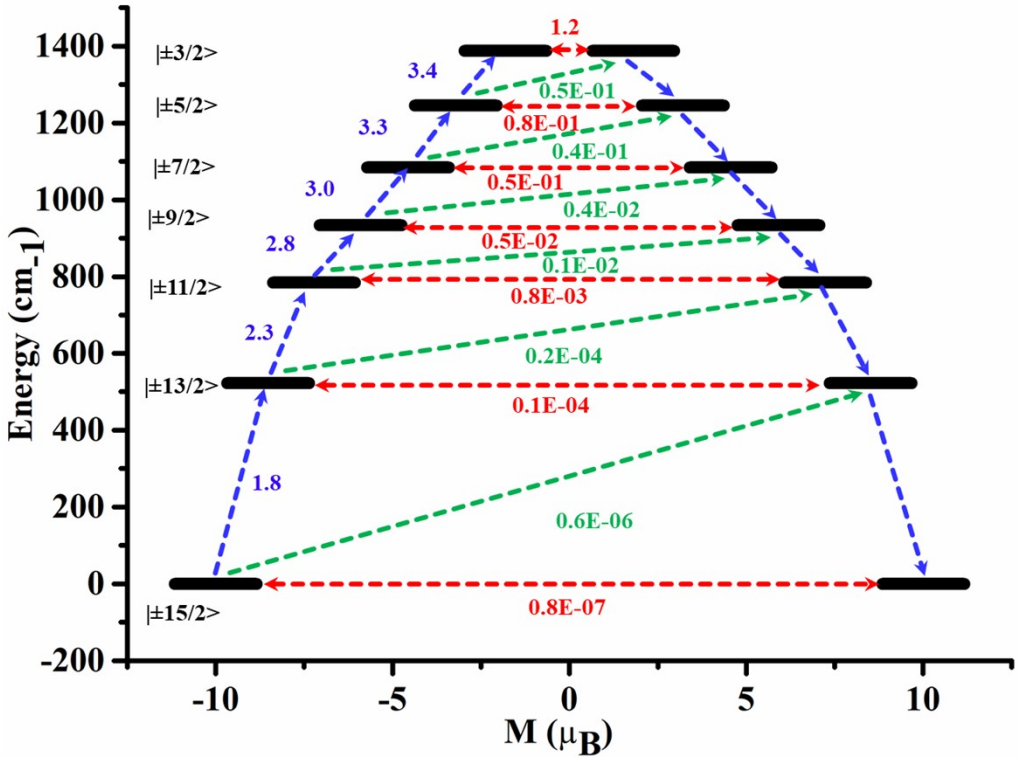

Figure S16. *Ab initio* computed magnetisation blockade barriers, along with computed transversal magnetic moments between the connecting pairs for **3-CA^{II}@CNT** .

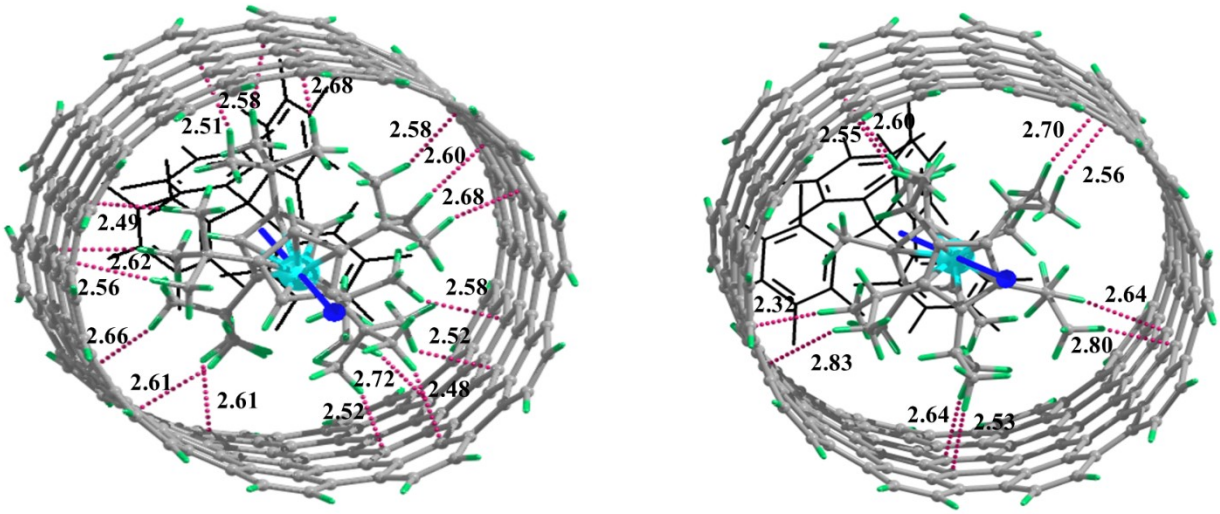

Figure S17. DFT optimized structures, Front view of a) **2-CA^{II}@CNT** b) **3^{II}@CNT**. Dotted purple lines show the closest C-H bond distances. Colour code: Dy^{III} - cyan, C- grey, and H- green. Blueline arrow shows the g_{zz} axis. In back, black colour chemdraw structure is counter anion $[B(C_6F_5)_4]^-$

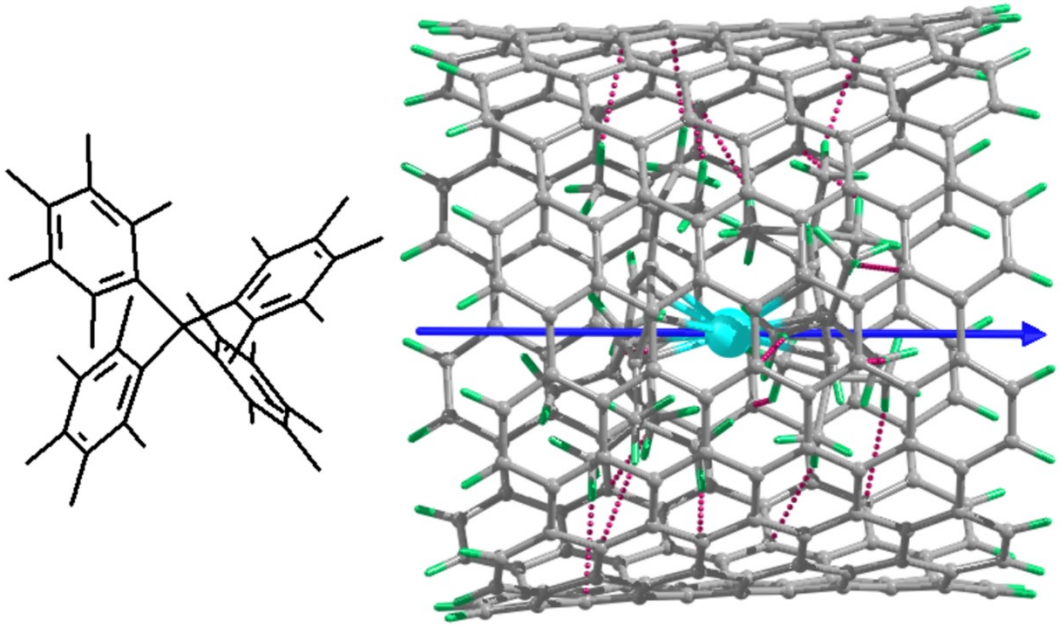

Figure S18. DFT optimized structures, Side view of a) **2-CA^{II}@CNT**. Dotted purple lines show the closest C-H bond distances. Colour code: Dy^{III} - cyan, C- grey, and H- green. Blueline arrow shows the g_{zz} axis. In back, black colour chemdraw structure is counter anion $[B(C_6F_5)_4]^-$

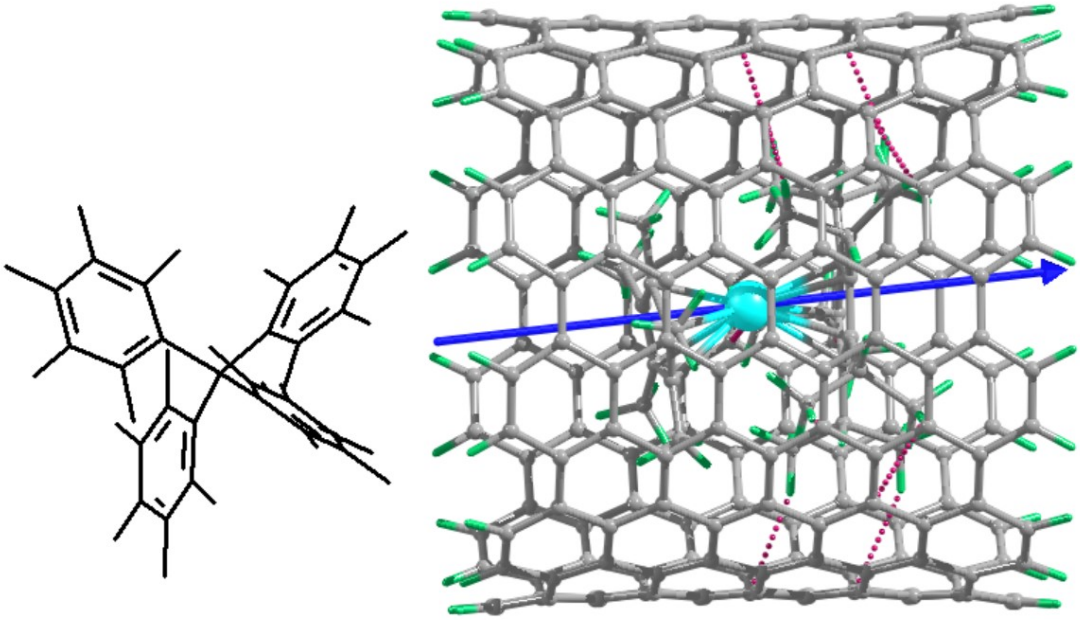

Figure S19. DFT optimized structures, Side view of a) **3-CA^{II}@CNT**. Dotted purple lines show the closest C-H bond distances. Colour code: Dy^{III} - cyan, C- grey, and H- green. Blueline arrow shows the g_{zz} axis. In back, black colour chemdraw structure is counter anion $[B(C_6F_5)_4]^-$

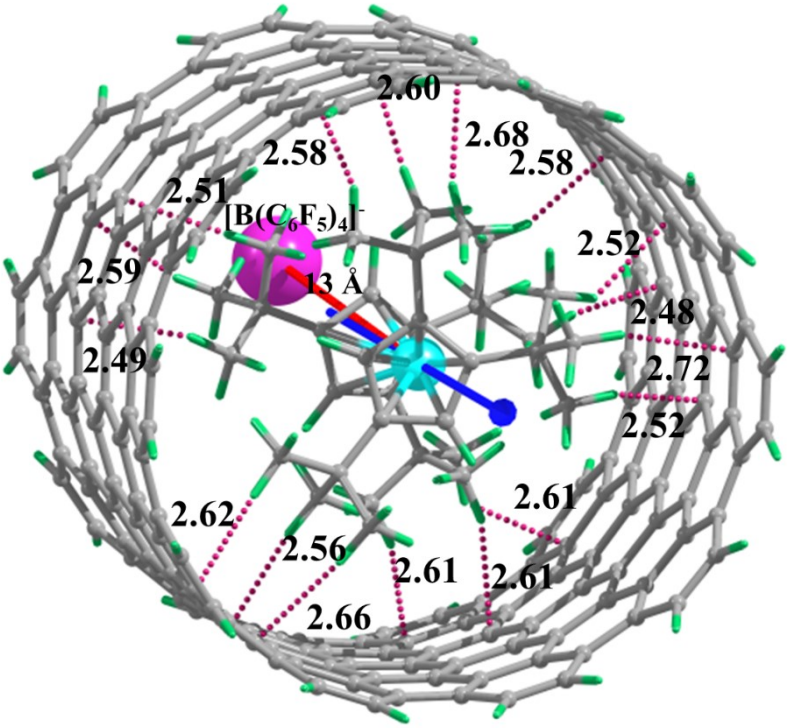

Figure S20. DFT optimized structures a) **3-CA^{II}@CNT** (see Fig. 1 for colour code and description). For visibility, $[B(C_6F_5)_4]^-$ is shown as a pink sphere.

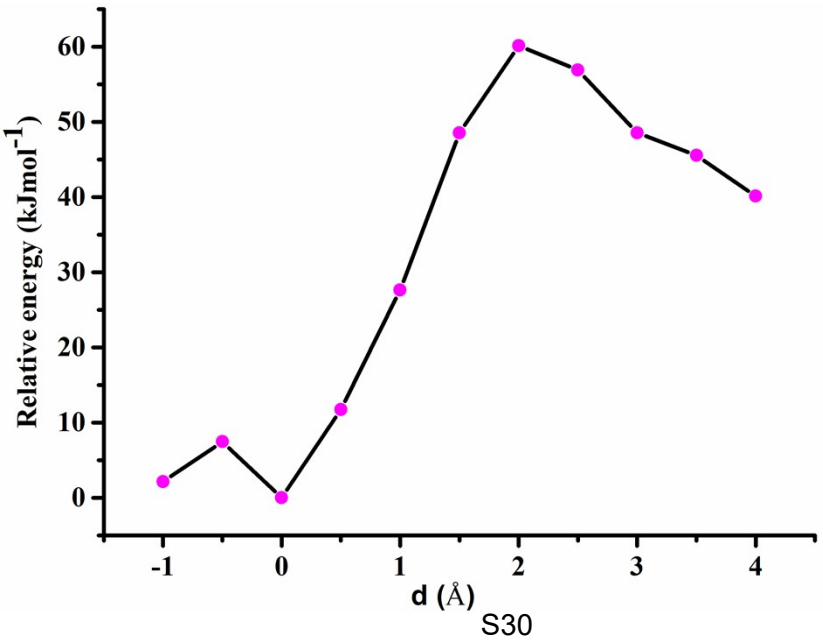

Figure S21. Relative energy vs displacement graph, when inside the CNT of **1**^{II}**@CNT**, the complex is displaced by 0.5 Å along the length of CNT.

References:

1. B. G. Lippert, J. H. PARRINELLO and MICHELE, *Mol. Phys.*, 1997, **92**, 477-488.
2. J. VandeVondele, M. Krack, F. Mohamed, M. Parrinello, T. Chassaing and J. Hutter, *Comput. Phys. Commun.*, 2005, **167**, 103-128.
3. T. D. Kühne, M. Iannuzzi, M. Del Ben, V. V. Rybkin, P. Seewald, F. Stein, T. Laino, R. Z. Khaliullin, O. Schütt and F. Schiffmann, *J. Chem. Phys.*, 2020, **152**, 194103.
4. G. Lippert, J. Hutter and M. Parrinello, *Theor. Chem. Acc.*, 1999, **103**, 124-140.
5. J. Paier, R. Hirschl, M. Marsman and G. Kresse, *J. Chem. Phys.*, 2005, **122**, 234102.
6. F. Aquilante, J. Autschbach, R. K. Carlson, L. F. Chibotaru, M. G. Delcey, L. De Vico, I. Fdez. Galván, N. Ferré, L. M. Frutos, L. Gagliardi, M. Garavelli, A. Giussani, C. E. Hoyer, G. Li Manni, H. Lischka, D. Ma, P. Å. Malmqvist, T. Müller, A. Nenov, M. Olivucci, T. B. Pedersen, D. Peng, F. Plasser, B. Pritchard, M. Reiher, I. Rivalta, I. Schapiro, J. Segarra-Martí, M. Stenrup, D. G. Truhlar, L. Ungur, A. Valentini, S. Vancoillie, V. Veryazov, V. P. Vysotskiy, O. Weingart, F. Zapata and R. Lindh, *J. Comput. Chem.*, 2016, **37**, 506-541.
7. T. H. Dunning and P. J. Hay, *Modern theoretical chemistry*, 1977, **3**, 1-28.
8. M. Frisch, G. Trucks, H. B. Schlegel, G. Scuseria, M. Robb, J. Cheeseman, G. Scalmani, V. Barone, B. Mennucci and G. Petersson, *Inc., Wallingford, CT*, 2009, **200**, 28.
9. J. Ogier, T. Arnauld and E. Doris, *Future medicinal chemistry*, 2009, **1**, 693-711.
10. S. Sun, S. Wang, S. Li, Y. Li, Y. Zhang, J. Chen, Z. Zhang, S. Fang and P. Wang, *Journal of Materials Chemistry A*, 2016, **4**, 18646-18653.
11. J. Kong, H. T. Soh, A. M. Cassell, C. F. Quate and H. Dai, *Nature*, 1998, **395**, 878-881.
12. A. Khorsand, S. Jamehbozorgi, R. Ghiasi and M. Rezvani, *Physica E: Low-dimensional Systems and Nanostructures*, 2015, **72**, 120-127.
13. M. Rezvani, M. D. Ganji and M. Faghihnasiri, *Physica E: Low-dimensional Systems and Nanostructures*, 2013, **52**, 27-33.